

1 AutoQS v1: Automatic parameterization of QuickSampling 2 based on training images analysis 3

4 Mathieu Gravey^{1,2,3}, Grégoire Mariethoz¹

5 ¹ [University](#) of Lausanne, Faculty of Geosciences and Environment, Institute of Earth Surface Dynamics,
6 Switzerland

7 ² [Institute for Interdisciplinary Mountain Research, Austrian Academy of Sciences, Innsbruck, Austria](#)

8 ³ [Department](#) of Physical Geography, Faculty of Geosciences, Utrecht University, Utrecht, Netherlands

9 Correspondence to: Mathieu Gravey (research@mgravey.com)

Deleted: ¹University

Deleted: ²Department

Deleted: research@mgravey.com

10 Highlights

- 12 • Adaptive calibration as a function of the simulation progression
- 13 • Calibration depends on each training image
- 14 • Robust parameterization based on a rapid prior analysis of the training image

Deleted: only

Deleted: the

15 **Abstract.** Multiple-point geostatistics are widely used to simulate complex spatial structures based on a training
16 image. The practical applicability of these methods relies on the possibility of finding optimal training images and
17 parametrization of the simulation algorithms. While methods for automatically selecting training images are
18 available, parametrization can be cumbersome. Here, we propose to find an optimal set of parameters using only
19 the training image as input. The difference between this and previous work that used parametrization optimization
20 is that it does not require the definition of an objective function. Our approach is based on the analysis of the errors
21 that occur when filling artificially constructed patterns that have been borrowed from the training image. Its main
22 advantage is to eliminate the risk of overfitting an objective function, which may result in variance underestimation
23 or in verbatim copy of the training image. Since it is not based on optimization, our approach finds a set of
24 acceptable parameters in a predictable manner by using the knowledge and understanding of how the simulation
25 algorithms work. The technique is explored in the context of the recently developed QuickSampling algorithm,
26 but it can be easily adapted to other pixel-based multiple-point statistics algorithms using pattern matching, such
27 as Direct Sampling or Single Normal Equation Simulation (SNESIM).
28

Deleted: use

Deleted: finding

Deleted: It

Deleted: The

Deleted: of our approach

Deleted: remove

Deleted: underestimating the

Deleted: a

29 1 Introduction

30 Geostatistics is extensively used in natural sciences to map spatial variables such as surface properties (e.g., soils,
31 geomorphology, meteorology) and subsurface geological features (e.g. porosity, hydraulic conductivity, 3D
32 geological facies). Its main applications involve the estimation and simulation of natural phenomena. In this paper,
33 we focus on simulation approaches.

Deleted: .

34 Traditional two-point geostatistical simulations preserve the histogram and variogram inferred from point data
35 (Matheron, 1973). However, inherent limitations make the reproduction of complex structures difficult (Gómez-
36 Hernández and Wen, 1998; Journel and Zhang, 2006). Multiple-point statistics (MPS), by accounting for more

Deleted: .

52 complex relations, enables the reproduction of such complex structures (Guardiano and Srivastava, 1993), but
 53 comes with its own limitations (Mariethoz and Caers, 2014). The main requirements for using MPS algorithms
 54 are 1) analog images (called training images) and 2) appropriate parametrization. While training images can often
 55 be provided by expert knowledge, and several methods have been proposed to automatically select one or a subset
 56 of appropriate training images among a set of candidates (Pérez et al., 2014; Abdollahifard et al., 2019). However,
 57 the parametrization of an MPS algorithm depends not only on the chosen training image but also on the specifics
 58 of the algorithm. This makes the task of finding good parametrization cumbersome, and therefore, users often have
 59 to resort to trial-and-error approaches (Meerschman et al., 2013). Here we will mainly focus on QuickSampling
 60 (QS) (Gravey and Mariethoz, 2020) which has as two main parameters: n that defines the maximum number of
 61 conditional data points to consider during the search process, and k which is the number of best candidates from
 62 which to sample the simulated value. Additionally, QS supports a kernel that allows weighting each conditioning
 63 pixel in the pattern based on its position related to the simulated pixel. Direct Sampling (DS) has for parameters:
 64 n which has an identical role as in QS, th that represents the pattern acceptance threshold, or the degree of
 65 similarity between local data patterns and the training image, and f the maximum proportion of the image that can
 66 be explored for each simulated pixel. In summary, n controls the spatial continuity, and k or th and f control the
 67 variability.

68 Over the last few years, several studies have addressed the challenge of automatically finding appropriate
 69 parameters for MPS simulation. These can be categorized in two approaches. The first approach is to assume that
 70 an optimal parametrization is related to the simulation grid (including possible conditioning data), the training
 71 image and the MPS algorithm. In this vein, Dagan et al. (2018) proposed a method that uses the known hard
 72 data from the simulation grid as a reference for computing the Jensen-Shannon divergence between histograms.
 73 Following this, they employ a simulated annealing optimization to update the MPS parameters until the metrics
 74 achieve the lowest divergence. This method is flexible enough to be adapted to any other metric. The second type
 75 of approach assumes that the parametrization is only related to the training image and the MPS algorithm. Along
 76 these lines, Baninajar et al. (2019) propose the MPS Automatic Parameter Optimizer (MPS-APO) method based
 77 on the cross-validation of the training image (TI) to optimize simulation quality and CPU cost. In this approach,
 78 artificially generated gaps in the high gradient areas of the training image are created, and a MPS algorithm is used
 79 to fill those gaps. The performance of a particular parameterization is quantified by assessing the correspondence
 80 between the filled and original training data. By design, this approach is extremely interesting for gap-filling
 81 problems. The authors state that it can be used for the parametrization of unconditional simulations; however, the
 82 use of limited gaps cannot guarantee the reproduction of long-range dependencies. Furthermore, due to the design
 83 of the framework for generating gaps, only MPS algorithms able to handle gap-filling problems can be used.
 84 While both approaches yield good results based on their objective functions, they all rely on a stochastic
 85 optimization process, therefore the duration of the optimization process cannot be predetermined or controlled by
 86 the user. Furthermore, an objective function is needed, which can be difficult because it depends on the training
 87 image used, many metrics can be accounted for in the objective function, such as histogram, variogram, pattern
 88 histogram, connectivity function, Euler characteristic, etc., (Boisvert et al., 2010; Renard and Allard, 2013; Tan et
 89 al., 2013) or a weighted combination of these. Similarly, one has to define meta-parameters linked to the
 90 optimization algorithm itself, such as the cooling rate in simulated annealing or maximum number of iterations.
 91 As a result, MPS parameter optimization approaches tend to be complex and difficult to use.

- Deleted: . However, MPS has
- Deleted: To perform satisfactorily,
- Deleted: require
- Deleted: Training
- Deleted: . Indeed, the training image is related to the property that is being simulated
- Deleted: therefore it is common to all MPS algorithms. In addition,
- Deleted: an
- Deleted:
- Deleted: , users often have to resort to a trial-and-error approaches (Meerschman et al., 2013)
- Deleted: good MPS
- Deleted: .
- Deleted: to
- Deleted: different philosophies.
- Deleted: categories
- Deleted: focused on the "simulation grid", which assumes
- Deleted: a
- Deleted: ,
- Deleted: using
- Deleted: to compute statistical metrics and then trying to improve the parametrization through
- Deleted: process
- Deleted: matched as closely as possible.
- Deleted: is focused on the "training image" and
- Deleted: d
- Deleted: quantify
- Deleted: algorithms are
- Deleted: simulate the
- Deleted: each
- Deleted: algorithm needs to be
- Deleted: for the error to be estimated properly
- Deleted: If
- Deleted: show
- Deleted: , then
- Deleted: are both related to
- Deleted: methods, and
- Deleted: , the user has no control over
- Deleted: .
- Deleted: . Finding this objective function is a challenge in itself
- Deleted: can change depending
- Deleted: . Using optimization approaches,
- Deleted: the

137 In this contribution, we propose a simplified optimization procedure for simulating complex systems. Rather than
138 using a complex optimization algorithm, our approach focuses on finding optimal parameters to accurately
139 simulate a single pixel in the system. The underlying principle of our approach is that if each pixel is accurately
140 simulated, the resulting sequence of pixels will converge to an accurate representation of the real-world system
141 being simulated. The goal is therefore to find the optimal parameters to simulate a single pixel using the training
142 image as the only reference. Baninajar et al. (2019) showed that computing the prediction error (i.e., the error
143 between the simulation and the reference) is an appropriate metric to identify optimal parameters. To find the
144 optimal parameters for simulating a single pixel, we propose an exhaustive exploration of the parameter space and
145 a computation of the prediction error between the simulation and the reference image.

146 The remainder of this paper is structured as follows: Section 2 presents the proposed method. Section 3 evaluates
147 the approach in terms of quantitative and qualitative metrics. Finally, section 4 discusses the strengths and
148 weaknesses of the proposed approach and presents the conclusions of this work.

149 2 Understanding and Addressing Verbatim Copy in Multiple Point Simulation

150 The principle underlying multiple point simulation is that the neighborhood of a given pixel x (the pattern
151 generated by known or previously simulated pixels) is informative enough to constrain the probability density
152 function of the value $Z(x)$. This requires a training image with several pattern repetitions. The Extended Normal
153 Equation Simulation (ENESIM) algorithm (Guardiano and Srivastava, 1993) computes the full probability
154 distribution for each simulated pixel. To ensure that enough samples are used, the SNESIM (Strebelle, 2002) and
155 the Impala (Straubhaar et al., 2011) algorithms include a parameter to define a minimum number of patterns
156 replicates. Direct Sampling (DS) (Mariethoz et al., 2010) adopts a different strategy by allowing for the interrupted
157 exploration of the training image. It includes a distance threshold parameter that defines what is an acceptable
158 match for a neighborhood, however, too small a threshold typically results in a single acceptable pattern in the
159 training image, leading to exact replication of parts of the training image, a phenomenon known as verbatim copy.
160 To reduce this issue, a parameter f is introduced controlling the fraction of the explored training image.
161 QuickSampling (QS) (Gravey and Mariethoz, 2020) also suffers from verbatim copy when the number of candidate
162 patterns is set to $k = 1$, the authors recommend the use of $k > 1$, and highlight that k is similar to the number of
163 replicates in SNESIM or IMPALA. A value $k = 1.5$ in QS can be seen as SNESIM with a minimum number of
164 replicates of 1 for 50% of the simulated values and 2 for the remaining values.

165 The definition of verbatim copy is the unintended pasting of a large section from the training image to the
166 simulation (patch-based approaches do so intentionally, e.g. (Rezaee et al., 2013)). This means that the relative
167 position of the simulated values is the same as that in the training image. This occurs when the neighborhood
168 constraints on the simulated pixels are too strong and only the exact same patterns as those in the training image
169 are acceptable. To detect this issue, a common strategy is to create a position map (similar to the index map),
170 which represents the provenance of simulated values by mapping their original coordinates in the training image,
171 as shown in Figure 1.

172 Figure 1 illustrates the most common forms of verbatim copy. The pure verbatim (the most common type of
173 verbatim copy) is a simple copy of a large part of the image, with all pixels in the same order inside of the patches.
174 Block verbatim typically appears when there are many replicates of a very specific type of pattern in the training
175 image and few replicates of all other patterns. Consequently, the MPS algorithm uses common patterns for

Deleted: skipping the complexity of an optimization algorithm and instead simplifying the ... simplified optimization procedure to a key element: the simulation of ... or simulating complex systems. Rather than using a complex optimization algorithm, our approach focuses on finding optimal parameters to accurately simulate a single pixel ... in the system. The underlying principle of our approach is that a ... f each pixel is accurately simulated, the resulting sequence of well-simulated ... ixels converges ... ill converge to a good simulation overall. Therefore, the ... n accurate representation of the real-world system being simulated. The goal is therefore to find the optimal parameters to simplify the simulation of ... imulate a single pixel using the training image as the only reference. Baninajar et al. (2019) showed that computing the prediction error (i.e., the error between the simulation and the reference) is an appropriate metric to find ... dentify optimal parameters. Following this approach ... o find the optimal parameters for simulating a single pixel, we propose exhaustively exploring an exhaustive exploration of the parameter space by performing pixel predictions over patterns extracted from the training image, ... nd compute ... computation of the associated ... rediction error. This results in a prediction error map for each combination of parameters (... [1])

Deleted: Section

Deleted: <#>Challenges related to inappropriate parameters#

Deleted: hypothesis behind ... rinciple underlying multiple point simulation is that the neighborhood of a given pix (... [2])

Deleted: $Z(x)$. Therefore, it

Deleted: enough repetition of the ... everal pattern (large enough) to allow the computation of such a conditional probability distribution. (... [3])

Deleted: algorithm ... omputes this ... he full probability distribution for the simulation of ... ach simulated pixel, therefore ensuring such a property ... To provide a similar guarantee ... nsure that enough samples are used, the SNESIM (Strebelle, 2002) algorithm ... nd the Improved Multiple-Point Parallel Algorithm using a List Approach (IMPALA) (... [4])

Deleted: ... algorithms include a parameter to define a minimum number of patterns replicates. Direct Sampling (DS) (Mariethoz et al., 2010) adopts a different strategy by allowing for the interrupted exploration of the training image. It includes a distance threshold parameter that defines what is an acceptable match for a neighborhood; however, too small a threshold typically results in a verbatim copy of the training image ... (... [5])

Deleted: To reduce this issue, a maximal fraction ... he definition of the explored training image is introduced, which is also called the exploration ratio. Since QuickSamplir (... [6])

Deleted: pixels

Deleted: Figure 1

Formatted: Font: 10 pt, Not Bold

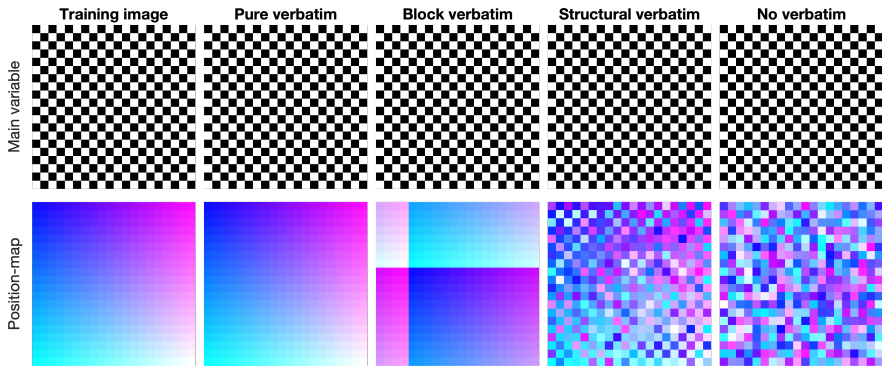
Field Code Changed

Deleted: Verbatim copy can appear in many forms; Figure 1

Deleted: shows ... llustrates the most common ones ... rms of verbatim copy. The pure verbatim (the most common type of verbatim copy) is a simple copy of a large part of the im (... [7])

Formatted: Font: 10 pt, Not Bold

350 transitioning between copied blocks resulting from rare patterns. Structural verbatim occurs when the copied
 351 portion spreads throughout the simulation without giving a direct impression of copying (e.g., pure verbatim over
 352 a subset of pixels). Structural verbatim tends to appear when large-scale structures are unique in the training image,
 353 which often allows a visually satisfying image to be quickly obtained, but with large non-stationary features
 354 identical to the training image. Often, users are willing to allow verbatim on large-scale structures, but this can
 355 easily introduce bias between simulations. This is one of the hardest types of verbatim to detect. Typically, this
 356 can occur when the maximum neighborhood radius is too large, leading to the duplication of large structures in
 357 the initial phase of the simulation. Finally, no verbatim, which is the expected result of simulations, occurs when
 358 the position of pixels does not have any particular structure (i.e. their position is unpredictable).



359
 360 **Figure 1** Visualization of verbatim copies using a position map. This is an extreme case that highlights that verbatim is
 361 not defined by the values simulated but by their position in the training image.

362 **3 Method**

363 The objective of the approach presented here is to find an optimal set of parameters using only the training image
 364 and knowledge of the simulation algorithm's mechanics. The simulation algorithm is not used in this context; in
 365 fact, simulations are not required to obtain a proper calibration, with the proposed method. The main target
 366 application of the presented approach is the pattern matching simulation algorithm QuickSampling (QS), where
 367 the values, at a pixel scale, are directly sampled from the training image. The method is suitable for the simulation
 368 of continuous and/or categorical variables.

369 Simulation algorithms such as QS, can be summarized by Algorithm 1. The key operation occurs at Line 3, which
 370 is when the algorithm searches for an optimal match based on the neighboring conditioning data.

371 **Algorithm 1** The sequential simulation algorithm. In gray the parametrization for QS.

- Deleted: is an example of
- Deleted: the white
- Deleted: .
- Deleted: .
- Deleted: ready
- Deleted: sacrifice
- Deleted: , which
- Deleted: This
- Deleted: typically
- Deleted: . We then perfectly duplicate
- Deleted: and
- Deleted: structure.
- Deleted: is
- Deleted: pixel
- Deleted: relations (

- Deleted: source of the value

- Deleted: approach
- Deleted: mechanics of the
- Deleted: algorithm as information
- Deleted: .

- Deleted: Binary variables are a particular case of continuous and categorical variables.
- Deleted: ,
- Deleted: Algorithm 1
- Deleted: QS

397
398 Inputs:
399 T : training images
400 S : simulation grid, including the conditioning data
401 P : simulation path
402 θ : parametrization,
403 n : number of neighbors
404 k : the number of best candidates
405 ω : the kernel, by default uniform

- 406 1. For each unsimulated pixel x following the path P :
- 407 2. Find the neighborhood $N(x)$ in S composed of the $n(\theta)$ closest neighbors
- 408 3. Find a candidate in T those matches $N(x)$ using the parametrization θ
- 409 4. Assign the value of the selected candidate to x in S
- 410 5. End

Deleted: (including n : number of neighbors)
Deleted: ¶
Deleted: using θ
Deleted: A

412 Here, we propose a divide and conquer approach that splits any pixel-based sequential simulation into its atomic
413 operation: the simulation of a single pixel. We assume that if all pixels are perfectly simulated, then the resulting
414 simulation should also be good. By a perfectly simulated pixel, we mean a pixel that respects the conditional
415 probability distribution. When simulating a pixel, there may be numerous potential valid values, but at the very
416 least, there should be one valid value, i.e., the conditional probability distribution should be represented in the
417 data. This can be formalized by the following condition:

$$|\{A|P(A|N(x)) > 0\}| \geq 1 \quad (1)$$

418 where $|\cdot|$ represents the cardinality of a set. $P(A|N(x))$ denotes the probability of A (a given value) knowing
419 $N(x)$, the neighborhood.

420 The proposed approach consists of finding a set of parameters that results in accurate samples for each pattern. At
421 the same time, we want to avoid systematically sampling perfect matches (the exact same neighborhood is
422 available in the training image), which results in a verbatim copy.

423 The search for the optimal parametrization is carried out by exhaustive exploration, and the choice of optimal
424 parameters is based on a prediction error defined as the difference between the original value of the pattern and
425 the value of the selected pattern in the training image.

426 **Algorithm 2**

428 Inputs:
429 D : list of stages of the simulation (i.e. pattern decimation levels, equivalent to fractions of the simulation path)
430 θ : list of discretized parameters
431 T the training images
432 \mathcal{V} a set of random positions (in practice we generated the random position on the fly)

- 433 1. For each possible combination of D and θ do for all $v \in \mathcal{V}$:
- 434 2. Sample a neighborhood $N(v)$ from T and decimate it according to stage D
- 435 3. Using θ , find a candidate in T that matches $N(v)$, excluding for v itself
- 436 4. Compute the error ε between the selected candidate and $Z(v)$
- 437 5. End
- 438 6. Analyze the errors ε to determine the best θ for each D_s

Deleted: applying
Deleted: by dividing
Deleted: A
Deleted: is
Deleted: Each possibility will still respect the probability distribution....
Deleted: An extreme and undesired situation occurs from
Deleted: simulation of a value that came from the
Deleted: of
Deleted: a simulation identical to the training image and therefore constitutes
Deleted: Algorithm 2). The
Deleted: is computed, which is
Deleted: pattern (Figure 2).
Moved (insertion) [1]
Moved (insertion) [2]
Moved (insertion) [3]
Moved (insertion) [4]

440 The proposed algorithm explores a discretized parameter space θ (Line 1) (e.g. for QS: n, k, ω). While this
441 discretization is natural for some parameters, such as n that is an integer, it can require an explicit discretization
442 for other parameters, such as the kernel in QS (or th in DS). Furthermore, a key component of our method is the
443 exploration of the parameter space for several representative stages D of the simulation (Line 1). In the case of a

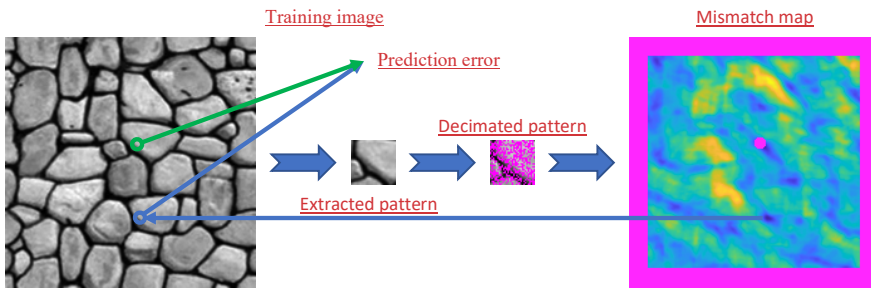
Deleted:
Deleted: Figure 2 All steps for a single pattern, summarizing Algorithm 2, Lines 2-4.
Deleted: Algorithm 2
Deleted:).
Deleted: potentially the
Deleted: Algorithm 2

469 random path, the progress of the simulation is directly related to the density of the neighborhoods, i.e., when $x\%$
 470 of the pixels are simulated, in average $x\%$ of neighbors are informed. To reproduce this behavior, at each stage D ,
 471 we randomly decimate patterns extracted from the TI by keeping only $x\%$ pixels informed. For each combination
 472 D and θ , multiple measures over a set of random locations \mathcal{V} ($500 < |\mathcal{V}| < 10000$) are computed in Lines 1-5 in
 473 with their mathematical expression shown in Equation 2:

$$474 \quad \varepsilon(\theta, D, T) = \sqrt{\frac{1}{|\mathcal{V}|} \sum_{\nu \in \mathcal{V}} \left(Z(\nu) - Z\left(\text{Cand}(\theta, N(\nu, D))\right) \right)^2} \quad (2)$$

475 where $\text{Cand}(\theta, N)$ returns a single candidate position for a given neighborhood N and follows the parametrization
 476 θ . $N(\nu, D)$ denotes a neighborhood around ν that is decimated according to stage D . \mathcal{V} represents a random set
 477 of positions in the training image, and $Z(\nu)$ refers to the actual value at position $\nu \in \mathcal{V}$ in the training image. To
 478 avoid parameters that generate verbatim copy of the training image, the position ν and its direct neighbors (in a
 479 small radius (here 5 pixels) are excluded from the set of potential candidates. The set of candidates considering
 480 this exclusion is denoted by $T \setminus \{\nu\}$ in Equation 2. Furthermore, in the case of equality between several optimal
 481 options, we set as a rule to take the cheapest parameter set in terms of computational cost (e.g., the smallest n),
 482 graphically represents the entire algorithm. Finally, for each stage considered, the set of parameters with the
 483 minimum associated error ε is considered optimal (Line 6):

$$484 \quad \varepsilon(\theta_{\text{optimal}}, D, T) = \min_{\theta} \varepsilon(\theta, D, T) \quad (3)$$



485 Figure 2 All steps for a single pattern, summarizing, Lines 2-4.
 486
 487

488 4 An efficient implementation

489 In practice, the implementation of Algorithm 2 separates θ into two parameter subsets: θ_h and θ_s . The θ_h subset
 490 consists of all parameters that influence the calculation of a single pattern match, which varies depending on the
 491 algorithm used. For instance, in QS, it includes the number of neighbors n and the kernel ω , while in DS, it
 492 comprises the threshold th and n . The other hand, θ_s encompasses parameters related to the sampling process of
 493 the training image. For QS, this includes the number of candidates to keep k , while for DS, it involves the fraction
 494 f of the training image being scanned.

- Deleted: ion
- Deleted: a
- Deleted: therefore D represents the density
- Deleted: a neighborhood
- Deleted: occur at
- Deleted: Algorithm 2 and
- Deleted: is
- Deleted: ,
- Deleted: ¶
- Deleted: decimated
- Deleted: respects the condition
- Moved (insertion) [5]
- Deleted: ¶
- Deleted: (in Algorithm 2, Line 6).
- Deleted: To avoid over-constrained situations from generating a verbatim copy of the training image, the position ν and its direct neighbors (in a small radius, usually around 5 pixels, but can we increase depending of the small scale structure of the training image) are removed from the set of potential candidates. Furthermore, in the case of equality between several optimal options, we propose the simple rules of taking the cheapest parameter set in terms of computational cost (e.g., ...
- Moved up [5]: the smallest n).
- Deleted: ¶
- Deleted: Algorithm 2 divides θ
- Deleted: of parameters
- Deleted: contains
- Deleted: the
- Deleted: affect
- Deleted: computation of the match
- Deleted: . This is dependent
- Deleted: ;
- Deleted: the case of
- Deleted: these are
- Deleted: ,
- Deleted: (
- Deleted: would be th ,
- Deleted: ,
- Deleted:).
- Deleted: includes the
- Deleted: In the case of
- Deleted: these are the number of matches to retain k ,
- Deleted: (and in the case of
- Deleted: f , which is
- Deleted: that is
- Deleted:). Interestingly, we can precompute

541 Our implementation precomputes and stores all matches for a specific θ_h parameterization (e.g., a value of n and
 542 all matches for k). Consequently, the saved matches of θ_h can be employed to swiftly evaluate all options for the
 543 parameters in $\theta = \theta_h \times \theta_s$ (e.g., we can process for $k = 1, 2, 3, \dots, k_{max}$). This two-phase approach considerably
 544 decreases redundant calculations.

545 The algorithm can be further accelerated by terminating the estimation of ϵ if the error remains at a high level after
 546 assessing only a small amount of samples from \mathcal{V} (here set to 500). To this end, we increase \mathcal{V} for the parameter
 547 combinations of interest, i.e., parametrization with potentially the lowest ϵ . This entails iterating and verifying at
 548 each step whether additional computations are required. Only places respecting following inequality are refined
 549 with extra measures:

$$\epsilon(\theta, D, T) - \epsilon(\theta_{min}, D, T) < \frac{1}{2}\sigma(\theta, D, T) + \frac{1}{2}\sigma(\theta_{min}, D, T) \quad (4)$$

551 With

$$\epsilon(\theta_{min}, D, T) = \min_{\theta} \epsilon(\theta, D, T)$$

$$\sigma(\theta, D, T) = \sqrt{\frac{1}{|\mathcal{V}|} \sum_{\nu \in \mathcal{V}} \left(Z(\nu) - Z\left(\underset{T(\nu)}{\text{Cand}}(\theta, N(\nu, D))\right) \right)^2 - \epsilon(\theta, D, T)}$$

554 With $\epsilon(\cdot)$ the error, and $\sigma(\cdot)$ represent the standard deviation of all differences, between estimated and true values.

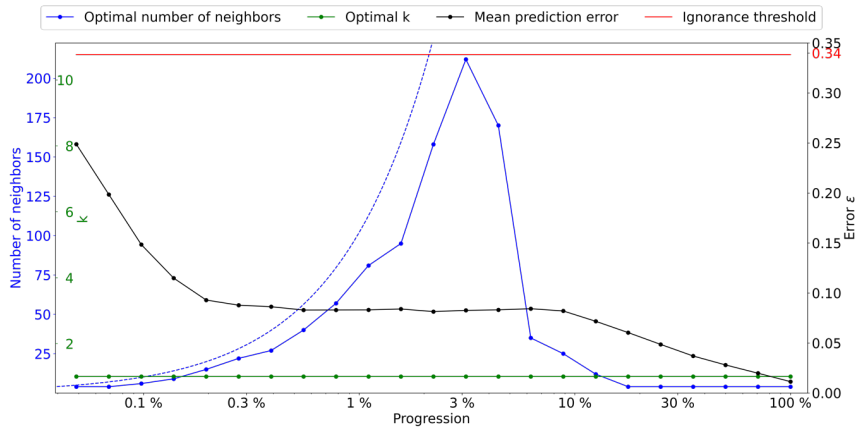
555 5 Results

556 5.1 Optimization of 2 parameters

557 All experimental tests in this section are performed using the training image shown in ν and the stages D are
 558 distributed following a logarithmic scale.

559 As a first test, we use the configuration $\theta_h = \{n\}$, and $\theta_s = \{k\}$. The kernel ω is defined as uniform, meaning that
 560 it has a constant value and is not part of the optimization. The outcome is represented in Figure 3, with the optimal
 561 number of candidates k and number of neighbors n as a function of the density D , which is assimilated to the
 562 progression during the simulation. The ignorance threshold is defined as the average error between elements of
 563 the marginal distribution. It represents the error value at which no further information can be derived from the
 564 neighborhood, meaning that the simulated values can equivalently be drawn from the marginal distribution.

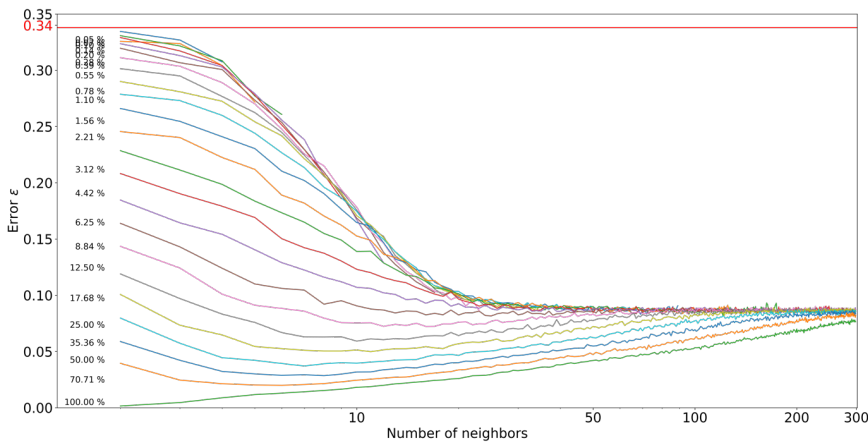
- Deleted: store of
- Deleted: given
- Deleted: θ_h . Then
- Deleted: used
- Deleted: quickly measure
- Deleted: possibilities
- Deleted: $\theta = \theta_h + \theta_s$.
- Deleted: step
- Deleted: allows to significantly reduce
- Deleted: computations. It is possible to
- Deleted: accelerate this algorithm
- Deleted: aborting
- Deleted: ϵ
- Deleted: having tested
- Deleted: number (at least 500)
- Deleted: .
- Deleted: carry out
- Deleted: last operation efficiently, the algorithm increases
- Deleted: . At
- Deleted: increase
- Deleted: , it checks if more
- Deleted: needed. The
- Deleted: rules proved a good trade-off
- Deleted: . Therefore, a given parametrization is only further explored if the error is a range of a σ .
- Deleted: <#>Result
- Deleted: Figure 2. The
- Deleted: Experimentation shows that the nodes simulated in the initial stages of the path are critical for the overall simulation
- Deleted: <#>Automatic calibration for QS
- In the case of QS, the method finds optimal values for k the number of candidates, n the number of neighbors and ω the kernel.
- Automatic calibration for QS with a uniform kernel
- In this
- Deleted: <#>results are shown
- Deleted: <#>Figure 3. It shows
- Deleted: <#> k
- Deleted: <#> progress (equivalent to the neighborhood density D).
- Deleted: <#>by computing
- Deleted: <#>beyond
- Deleted: <#>is extracted
- Deleted: <#>stage where
- Deleted: <#>then
- Deleted: <#> without introducing bias



612
613 **Figure 3** Optimal parameters for QS (k in green and number of neighbors in blue) as a function of the progression,
614 with the associated prediction error (in black). The red line represents the ignorance threshold. The dashed blue line
615 indicates the average maximal number of neighbors.

616
617 The optimal k remains small (in fact 1) throughout the simulation, which is probably due to the limited size of the
618 training image in this case. It seems important to use many neighbors in the early stages of the simulation. The
619 number of neighbors increases until approximately 3% of the simulation. This is followed by a subsequent drastic
620 reduction, indicating that once the large structures are informed, only the few direct neighbors are important. It
621 seems logical that MPS algorithms simulate large structure first and then smaller patterns in a hierarchical manner
622 where each smaller structure is part of the larger one. We however note that it remains generally difficult to predict
623 the optimal settings as a function of the simulation stage. This indicates that the use of a single parametrization for
624 the entire MPS simulation is generally suboptimal, and the parameters should be adapted as the simulation
625 progresses.

- Deleted: density for the neighborhood considered.
- Deleted: k
- Deleted: because
- Deleted: is not sufficiently repetitive (large). At early stages of the simulation, it
- Deleted: .
- Deleted: .
- Deleted: . This tends to indicate
- Deleted: We also
- Deleted: even if the parametrization is logical, it is
- Deleted: .
- Deleted: . Figure 3 also shows that the first few simulated pixels are hardly predictable (close to the ignorance threshold)...



626
627 **Figure 4** Pattern error as a function of the number of neighbors n , with $k = 1$, where each curve represents a
628 neighborhood density D .

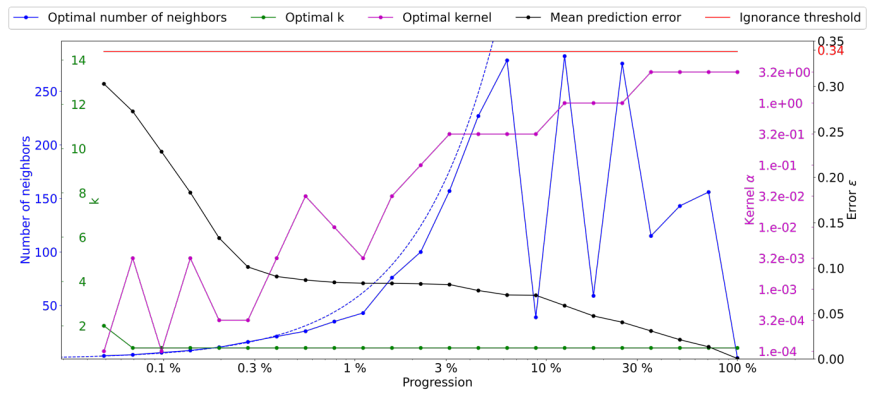
- Deleted: Error
- Deleted: ←
- Deleted: the associated density of the

646
 647 **Figure 4** shows the evolution of ϵ as a function of the number of neighbors n and the simulation progression D .
 648 **Two regimes are visible:** in the first percentages of the simulation, **each extra neighbor is informative and improves**
 649 **simulation quality.** However, as the neighborhoods become denser, the importance of spatial continuity takes over,
 650 **and only the few neighbors are really informative.** This two-step process is expected, as random large-scale
 651 features are generated first, **and then the image is filled** with consistent fine-scale structures. Furthermore, it shows
 652 that using a large number of neighbors at the end of the simulation generates suboptimal results, which could
 653 explain the small-scale noise that is sometimes visible in some MPS simulations.
 654

Deleted: Figure 4
 Deleted: in
 Deleted: stage. This indicates that two
 Deleted: exist
 Deleted: simulation. In the
 Deleted: an optimal prediction can be obtained even with a
 Deleted: small number of neighbors.
 Deleted: .
 Deleted: ; then, in a second step, the MPS algorithm fills
 Deleted: a

655 **5.2 Optimization of 3 parameters**
 656 Here, we use the following configuration $\theta_h = \{n, \alpha\}$ and $\theta_s = \{k\}$, and we consider kernels as having a radial
 657 exponential shape, i.e. $\omega_i = e^{-\alpha d_i}$. The weight of a given position i in the kernel ω is defined as ω_i , and its distance
 658 to the kernel center as d_i .

Deleted: Automatic calibration of QS considering
 Deleted: different kernels
 Deleted: $\{n, \omega\}$
 Deleted: . We
 Deleted: w_i

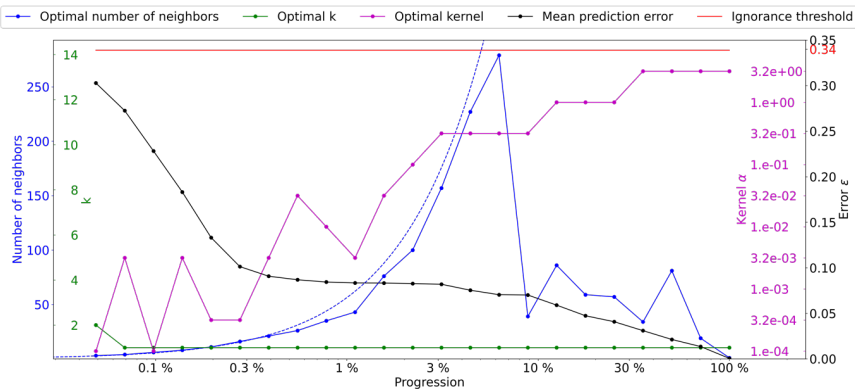


659 **Figure 5** Optimal parameters for QS (k in green, number of neighbors in blue, and best kernel in magenta), as a function
 660 of the **simulation progress**, with the associated prediction error (in black). The dashed blue line indicates the average
 662 density for the neighborhood considered. **The ignorance threshold in red.**

Deleted:)
 Deleted: progression
 Moved (insertion) [6]
 Deleted: Figure 5
 Deleted: shows
 Deleted: evolution
 Deleted: QS parameters, where interferences between the
 Deleted: skewed
 Deleted: α are visible. This interaction
 Deleted: explained by the fact
 Deleted: last
 Deleted: will receive
 Deleted: weights
 Deleted: α
 Deleted: and thus n becomes insensitive. In that case, the
 Deleted: are negligible, with random
 Deleted: ;
 Deleted: This tolerance
 Deleted: introduced
 Deleted: extra
 Deleted: for example
 Deleted: When
 Deleted: gain
 Deleted: s
 Deleted: , up
 Deleted: a
 Deleted: % computational gain was observed using Equation
 Deleted: 4...

663
 664 **The results presented in Figure 5 demonstrate the impact of the number of neighbors and narrow kernels**
 665 **(characterized by high α values) on the evolution of the QS parameters. Specifically, it can be observed that**
 666 **interactions arise between these two factors, resulting in slightly erratic calibrated parameters. As the number of**
 667 **neighbors increases, the weights assigned to the furthest neighbors become negligible with larger α values. This**
 668 **means that these far away neighbors, despite being considered, have very little influence. This insensitivity only**
 669 **occurs for large n values, leading to minimal differences between possible configurations and noise in the metric.**
 670 As expressed in the methodology section, in cases of a similar error, the cheapest solution is considered. In the
 671 case of QS, having a large number of neighbors can marginally increase the computational time, therefore, we
 672 introduce a small tolerance that results in favoring small n values. It is formulated as a small cost for each extra
 673 neighbor, i.e., by adding $5e-5 \times (\max(T) - \min(T))$ for each extra neighbor. However, the speed-up during
 674 simulation was limited to up to 10%. Figure 6 shows similar quality (ϵ curves) as in Figure 5, but with the added

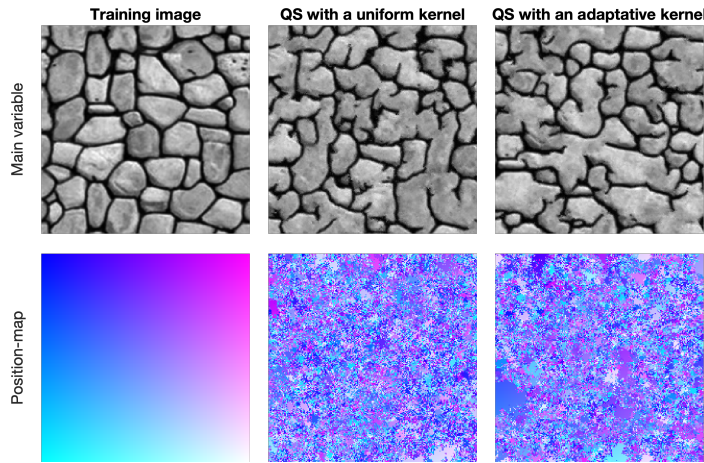
717 tolerance. As expected, the number of neighbors required during the simulation drastically decreases as advanced
 718 simulation stages, and the fluctuations in n are avoided.



719
 720 **Figure 6** Optimal parameters for QS (k in green and number of neighbors in blue, and the best kernel in magenta)
 721 as a function of the progression, with the associated prediction error (in black). The dashed blue line is the average
 722 density for the neighborhood considered. The ignorance threshold is in red.

723 **5.3 Sequential simulation using automatic calibration**

724 Figure 7 shows qualitative results using the evolutive parametrization resulting of the proposed autocalibration,
 725 using a case study that was published in Gravey and Mariethoz (2020). QS with an adaptive kernel refers to the
 726 use of different values of α for the kernel as a function of the simulation progression. In this case, the results are
 727 similar to state-of-the-art simulations using a manual calibration. Tests using QS with a uniform kernel fail to
 728 reproduce some structures, in particular, the size of the objects is incorrect. Each position-map shows few
 729 homogenous areas; therefore, realizations are produced with a low rate of verbatim copy.

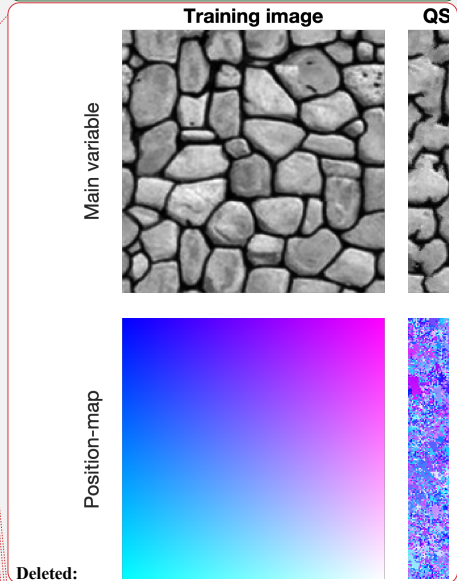


730
 731 Figure 7 Simulation using QS with parameters generated by the automatic calibration.
 732

Deleted: ¶

Deleted: Figure 6 shows similar quality (ϵ curves) as Figure 5. However, the number of neighbors required during the simulation drastically decreases as advanced simulation stages, and the wild oscillations are avoided. ¶

Moved down [7]: Figure 7 Simulation using QS with parameters generated by the automatic calibration. ¶



Deleted:

Deleted: Figure 7

Deleted: .

Deleted: alpha

Deleted: ;

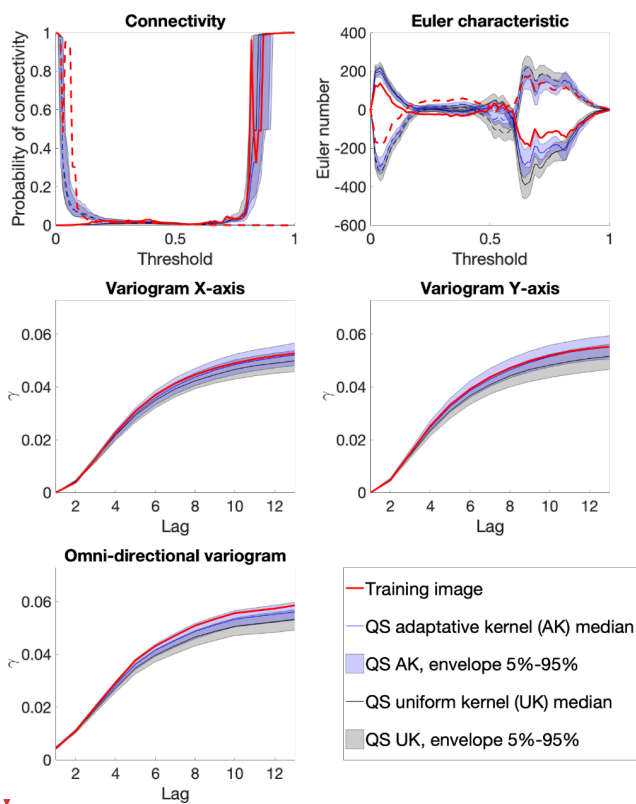
Deleted: ,

Deleted: verbatim

Moved (insertion) [7]

747 From a quantitative evaluation, Figure 8 illustrates different metrics (variograms, connectivity as a structural
 748 indicator, and the Euler characteristic as noise indicator) (Renard and Allard, 2013) across a set of 100 realizations.
 749 The automatic calibration method proposed here allows obtaining better quality simulations than in Gravey and
 750 Mariethoz (2020).
 751 Figure 9 shows that variogram and connectivity metrics are well reproduced, although they have not been directly
 752 constrained in the calibration process. Indeed, the parameter optimization only considers the simulation of single
 753 pixels and never computes global metrics over an entire grid.
 754

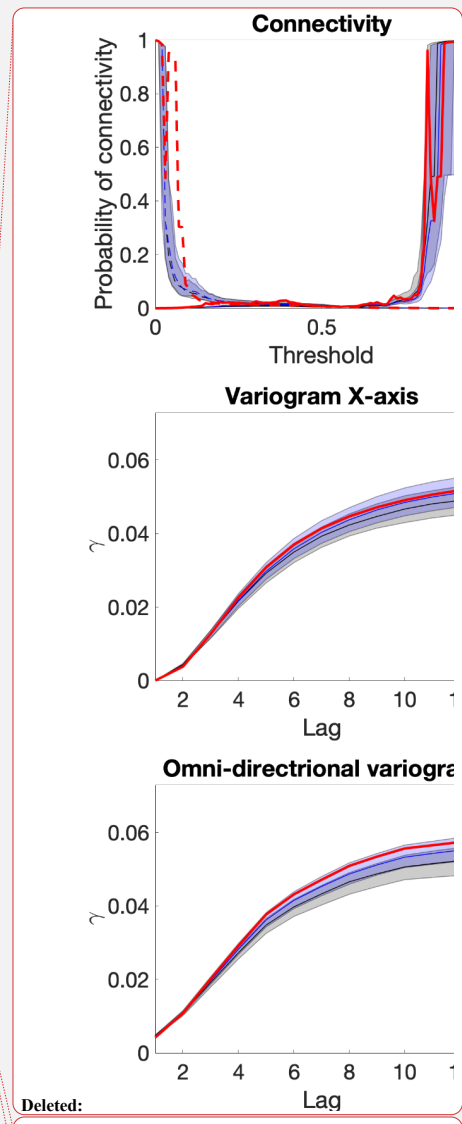
Deleted: point of view
 Deleted: Figure 8
 Deleted: simu
 Deleted: for
 Deleted: the original QS article.



755 **Figure 8 Benchmark between QS with an adaptive kernel (Figure 6) and a uniform (without) kernel (Figure 3) over 100**
 756 **simulations for 5 different metrics.**
 757

758 **6 Discussion and conclusion**

759 The proposed method allows for the automatic calibration of QS and potentially similar pixel-based MPS
 760 approaches, reaching a similar or better quality as that of manual parameterization from both quantitative and
 761 qualitative points of view. Furthermore, it demonstrates that the optimal parametrization should not remain
 762 constant and instead needs to evolve with the simulation progression. The metrics confirm the good reproduction



Deleted:
 Deleted: Figure 6
 Deleted: Figure 3

771 of training patterns and the method finds a calibration that avoids verbatim copy. One major advantage of our
 772 approach is the absence of a complex objective function, which often itself requires calibration.
 773 A limitation of our approach is that it cannot be used to determine an optimal simulation path because it focuses
 774 on the simulation of a single pixel. It also does not optimize the computational cost required for a simulation.
 775 The computation time necessary to identify the appropriate parameters is contingent upon the expected quality.
 776 However, the maximum time required for completion is predictable and depends on the number of patterns tested.
 777 If required, the calibration can be further refined based on prior outcomes without restarting the entire process;
 778 this can be achieved by adjusting D , incorporating additional kernels, or increasing $|\mathcal{V}|$. In certain instances,
 779 adjusting the kernel parameter offers only minor improvements while necessitating a substantial number of
 780 computations. Employing a more streamlined parameter space can yield comparable, and significantly reduce the
 781 computational cost. This streamlined parameter space can be established, for instance, by subsampling the number
 782 of neighbors according to a squared function (2,4,9,16,25,...) or by leveraging external or expert knowledge.
 783 The proposed methodology was evaluated in multivariate scenarios, resulting in a more expansive parameter space
 784 compared to single-variable cases. Although the approach yields satisfactory parameters, the inclusion of extra
 785 parameters significantly extends the computation time, rendering the process impractical, particularly when
 786 dealing with four or more variables.
 787 In the context of testing the generality of our approach, calibration was computed on multiple training images
 788 (found in the Supplementary material). The calibration pattern with two regimes (n large, then n small) seems to
 789 be universal, at least for univariate simulations. While the position of the abrupt transition between regimes seems
 790 to vary greatly (between 0.5% and 20% of the path), the overall shape remains the same. Therefore, the approach
 791 proposed by Baninajar et al. (2019), in which long ranges are not considered, could be extended by using large n
 792 values in the early stages of the simulation.
 793 While show that it is possible to calibrate a parametric kernel, in future work one can envision the optimization of
 794 a nonparametric kernel where the weight of each individual neighbor w_i is considered a variable to optimize using
 795 ϵ as an objective function (e.g., using a machine learning regression framework).
 796 The study of the evolution of parameters shows a smooth behavior of the average error. Therefore, the use of
 797 multivariate fitting approaches to estimate the error surface with fewer evaluations could be an interesting solution
 798 to speed up the parametrization. The use of machine learning to take advantage of transfer learning between
 799 training images also has a high potential.

801 **Code availability**

802 The source code of the AutoQS algorithm is available as part of the G2S package at: [https://github.com/GAIA-](https://github.com/GAIA-UNIL/G2S)
 803 [UNIL/G2S](https://github.com/GAIA-UNIL/G2S) (last access: 1st May 2023) under the GPLv3 license. And permanently available at
 804 <https://doi.org/10.5281/zenodo.7792833>. Platform: Linux/macOS/Windows 10+. Language: C/C++. Interfacing
 805 functions in MATLAB, Python3, and R.

806 **Author contributions.**

807 MG proposed the idea, implemented and optimized the autoQS approach and wrote the article. GM provided
 808 supervision, methodological insights and contributed to the redaction.

- Deleted:** because...nd the method finds a calibration that avoids verbatim copy.¶
The...One major advantage of our approach is the absence of a complex objective function, which often itself requires calibration. The method runs in a predictable maximum time, which depends of the number of patterns tested, that relate on the expected quality of the calibration σ . The calibration can even be refined based on previous results, without running all the processes again, by adding steps, kernels, or by increasing $|\mathcal{V}|$. (... [8])
- Deleted:** Our... limitation of our approach is that it cannot be used to determine an optimal simulation path because it focuses on the simulation of a single pixel. Furthermore, the method...t also does not take into consideration (... [9])
- Deleted:** of...ecessary to identify the optimal...ppropriate parameters depends on...s contingent upon the expected quality. For example, sometimes a (... [10])
- Deleted:** provides...arameter offers only a small improvement but requires many...minor improvements while necessitating a substantial number of computations. A full exploration of a 250x250 image takes approximately 30 min. However, a result using a degraded...mploying a more streamlined parameter space can provide close results in less than 10 min...ield comparable, and significantly reduce the computational cost. This degraded...reamlined parameter space can be constructed...stablished, for example...nstance, by subsampling the number of neighbors following...ccording to a squared function or using some...2,4,9,16,25,...) or by leveraging external/ (... [11])
- Deleted:** method...roposed methodology was explored for multivariable images, ...valuated in multivariate scenarios, resulting in a larger parametrization...ore expansive parameter space than with a...ompared to single...variable. The method provides good results independent of the task. Unfortunately, when performing this ...cases. Although the approach, each new parameter increases...ields satisf (... [12])
- Deleted:** the proposed...ur approach, calibration was computed on multiple training images (found in the Appendix B, C). Unexpectedly, the (... [13])
- Deleted:** er... seems to be universal, at least for single variable...nivariate simulations. While the position of the abrupt transition between each regime...egimes seems to vary greatly (between 0.5% and 20% of the path), the over (... [14])
- Moved up [6]:** <#>¶
The
- Deleted:** <#>Conclusion¶
The proposed approach allows for the automatic calibration of pixel-based MPS algorithms. Furthermore, it demonstrates that for optimal results, the parametriz (... [15])
- Deleted:** <#>proposed method allows for the calibration of a parametric kernel. However
- Deleted:** <#>frameworks
- Deleted:** a...multivariate fitting approaches to estimate the error surface with fewer evaluations could be an interesting solution to speed up the parametrization by capitalizing on neighbors (in parameter space)... The use of machine (... [16])
- Deleted:** a...utoQS algorithm is available as part of the G2S package at: <https://github.com/GAIA-UNIL/G2S>...HYPERLINK "https://github.com/GAIA (... [17])
- Deleted:** writing of the article

1040 **Competing interests**

1041 The authors declare that they have no conflict of interest.

1042 **Acknowledgements**

1043 This research was funded by the Swiss National Science Foundation.

1044 **6.1 Financial support**

1045 This research has been supported by the Swiss National Science Foundation (grant no. 200021_162882).

1046 **7 References**

- 1047 Abdollahifard, M. J., Baharvand, M., and Mariétoz, G.: Efficient training image selection for multiple-point
1048 geostatistics via analysis of contours, *Computers & Geosciences*, 128, 41–50,
1049 <https://doi.org/10.1016/j.cageo.2019.04.004>, 2019.
- 1050 Baninajar, E., Sharghi, Y., and Mariétoz, G.: MPS-APO: a rapid and automatic parameter optimizer for multiple-
1051 point geostatistics, *Stoch Environ Res Risk Assess*, 33, 1969–1989, <https://doi.org/10.1007/s00477-019-01742-7>,
1052 2019.
- 1053 Boisvert, J. B., Pyrez, M. J., and Deutsch, C. V.: Multiple Point Metrics to Assess Categorical Variable Models,
1054 *Nat Resour Res*, 19, 165–175, <https://doi.org/10.1007/s11053-010-9120-2>, 2010.
- 1055 Dagan, Y., Renard, P., Straubhaar, J., Erten, O., and Topal, E.: Automatic Parameter Tuning of Multiple-Point
1056 Statistical Simulations for Lateritic Bauxite Deposits, *Minerals*, 8, 220, <https://doi.org/10.3390/min8050220>, 2018.
- 1057 [Gómez-Hernández, J. J. and Wen, X.-H.: To be or not to be multi-Gaussian? A reflection on stochastic](#)
1058 [hydrogeology, *Advances in Water Resources*, 21, 47–61, \[https://doi.org/10.1016/s0309-1708\\(96\\)00031-0\]\(https://doi.org/10.1016/s0309-1708\(96\)00031-0\), 1998.](#)
- 1059 Gravey, M. and Mariétoz, G.: QuickSampling v1.0: a robust and simplified pixel-based multiple-point simulation
1060 approach, *Geosci. Model Dev.*, 13, 2611–2630, <https://doi.org/10.5194/gmd-13-2611-2020>, 2020.
- 1061 Guardiano, F. B. and Srivastava, R. M.: Multivariate Geostatistics: Beyond Bivariate Moments, in: *Quantitative*
1062 *Geology and Geostatistics*, Springer Netherlands, 133–144, https://doi.org/10.1007/978-94-011-1739-5_12, 1993.
- 1063 [Journel, A. and Zhang, T.: The Necessity of a Multiple-Point Prior Model, *Math Geol*, 38, 591–610,](#)
1064 <https://doi.org/10.1007/s11004-006-9031-2>, 2006.
- 1065 [Mahmud, K., Mariétoz, G., Caers, J., Tahmasebi, P., and Baker, A.: Simulation of Earth textures by conditional](#)
1066 [image quilting, *Water Resour. Res.*, 50, 3088–3107, <https://doi.org/10.1002/2013wr015069>, 2014.](#)
- 1067 Mariétoz, G., Caers, J., 2014. *Multiple-point geostatistics: stochastic modeling with training images*. Wiley.
- 1068 Mariétoz, G., Renard, P., and Straubhaar, J.: The Direct Sampling method to perform multiple-point geostatistical
1069 simulations, *Water Resour. Res.*, 46, <https://doi.org/10.1029/2008wr007621>, 2010.
- 1070 Matheron, G.: The intrinsic random functions and their applications, *Advances in Applied Probability*, 5, 439–
1071 468, <https://doi.org/10.2307/1425829>, 1973.
- 1072 Meerschman, E., Pirot, G., Mariétoz, G., Straubhaar, J., Van Meirvenne, M., and Renard, P.: A practical guide
1073 to performing multiple-point statistical simulations with the Direct Sampling algorithm, *Computers &*
1074 *Geosciences*, 52, 307–324, <https://doi.org/10.1016/j.cageo.2012.09.019>, 2013.

1075 Pérez, C., Mariethoz, G., and Ortiz, J. M.: Verifying the high-order consistency of training images with data for
1076 multiple-point geostatistics, *Computers & Geosciences*, 70, 190–205,
1077 <https://doi.org/10.1016/j.cageo.2014.06.001>, 2014.

1078 Renard, P. and Allard, D.: Connectivity metrics for subsurface flow and transport, *Advances in Water Resources*,
1079 51, 168–196, <https://doi.org/10.1016/j.advwatres.2011.12.001>, 2013.

1080 Rezaee, H., Mariethoz, G., Koneshloo, M., and Asghari, O.: Multiple-point geostatistical simulation using the
1081 bunch-pasting direct sampling method, *Computers & Geosciences*, 54, 293–308,
1082 <https://doi.org/10.1016/j.cageo.2013.01.020>, 2013.

1083 Straubhaar, J., Renard, P., Mariethoz, G., Froidevaux, R., and Besson, O.: An Improved Parallel Multiple-point
1084 Algorithm Using a List Approach, *Math Geosci*, 43, 305–328, <https://doi.org/10.1007/s11004-011-9328-7>, 2011.

1085 Strebelle, S.: *Mathematical Geology*, 34, 1–21, <https://doi.org/10.1023/a:1014009426274>, 2002.

1086 Tan, X., Tahmasebi, P., and Caers, J.: Comparing Training-Image Based Algorithms Using an Analysis of
1087 Distance, *Math Geosci*, 46, 149–169, <https://doi.org/10.1007/s11004-013-9482-1>, 2013.

1088

1089

1090

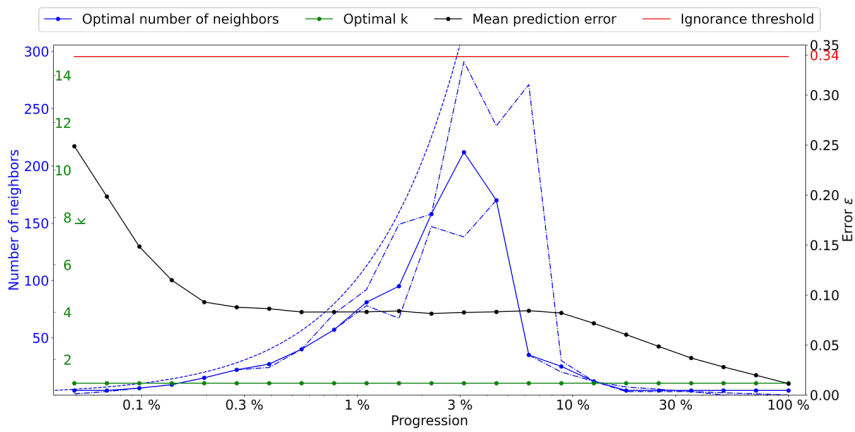
Deleted:Section Break (Continuous).....

Appendix

1092
1093
1094

This supplementary material contains a similar calibration for other training images.

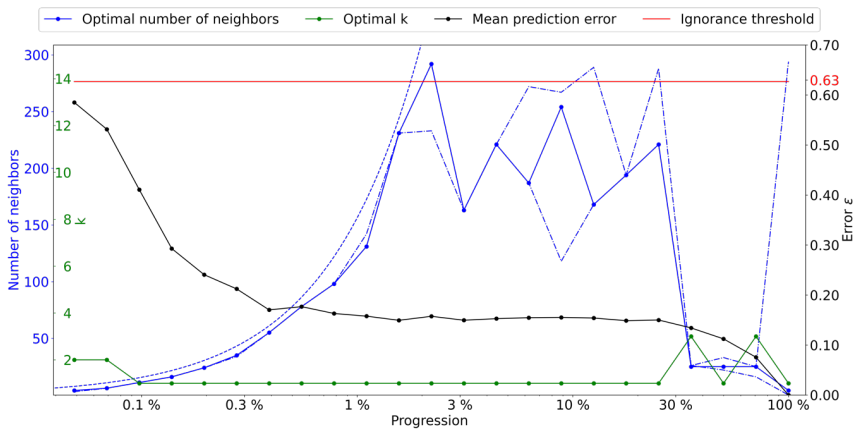
1095 A. Stone



1096
1097
1098
1099

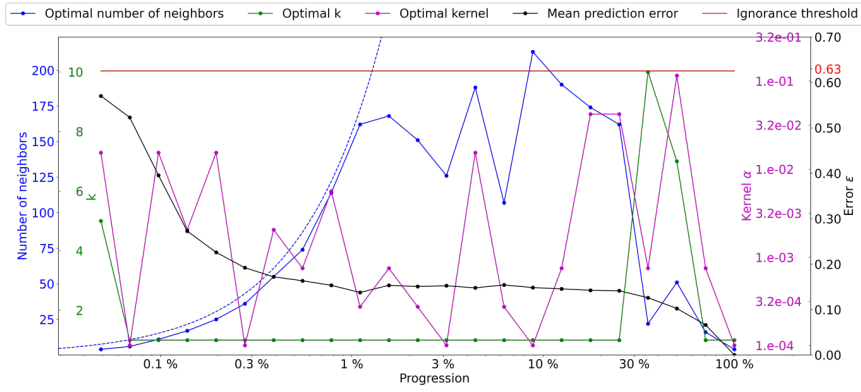
Figure A.1 Optimal parameters for QS (k in green and number of neighbors in blue) as a function of the progression, with the associated prediction error (in red). The red line represents the ignorance threshold. The dashed blue line is the average density for the neighborhood considered. The dot-dashed line represents the variability in 1% of the error.

1100 B. Strebelle (Strebelle, 2002)

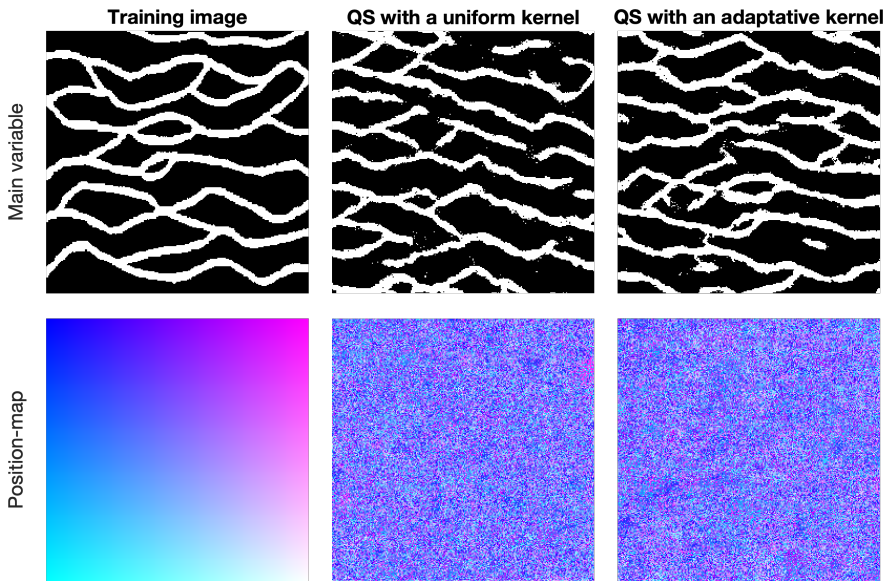


1101
1102
1103
1104

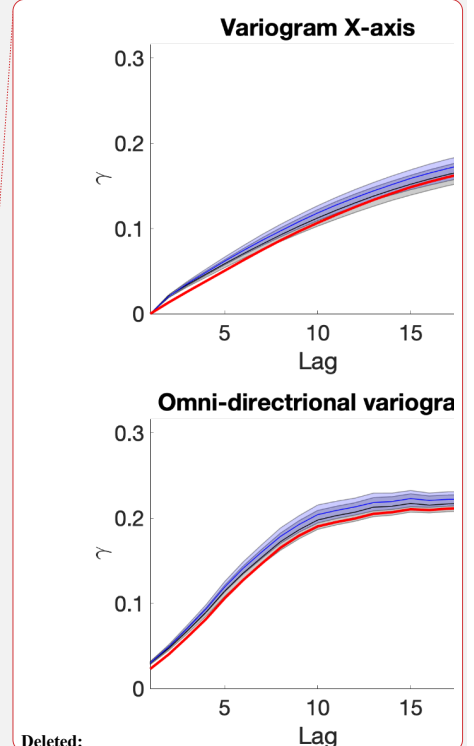
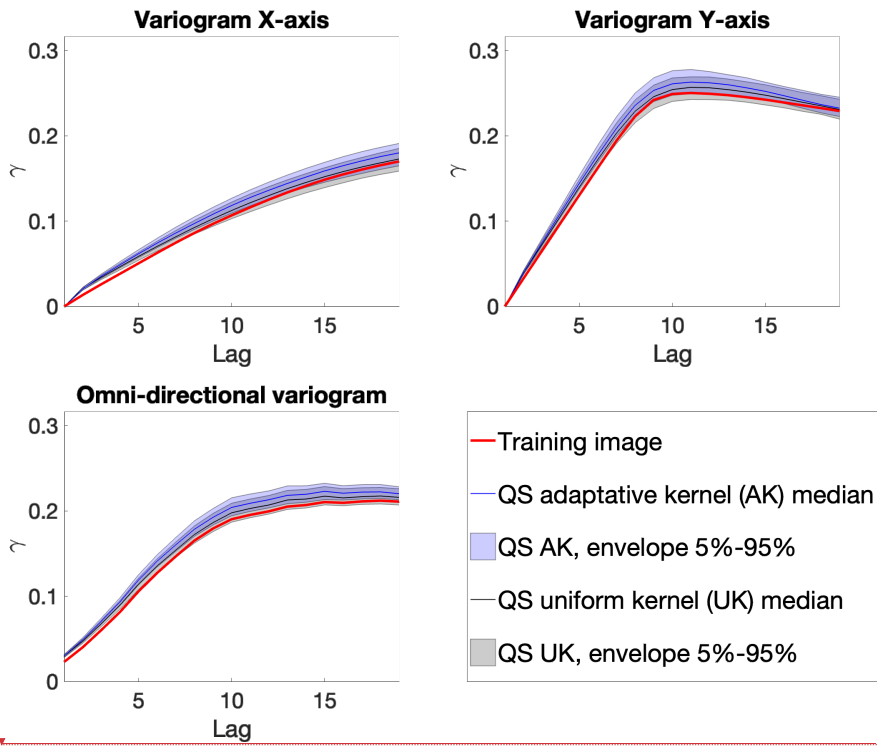
Figure B.1 Optimal parameters for QS (k in green and number of neighbors in blue) as a function of the progression, with the associated prediction error (in red). The red line represents the ignorance threshold. The dashed blue line is the average density for the neighborhood considered. The dot-dashed line represents the variability in 1% of the error.



1105
 1106 **Figure B.2** Optimal parameters for QS (k in green and number of neighbors in blue, and the best kernel in magenta)
 1107 as a function of the progression, with the associated prediction error (in red). The dashed blue line is the average density
 1108 for the neighborhood considered.



1109
 1110 **Figure B.3** Simulation using QS using parameters generated by the automatic calibration.



Deleted:

Deleted: Figure B.2

Deleted: Figure B.1

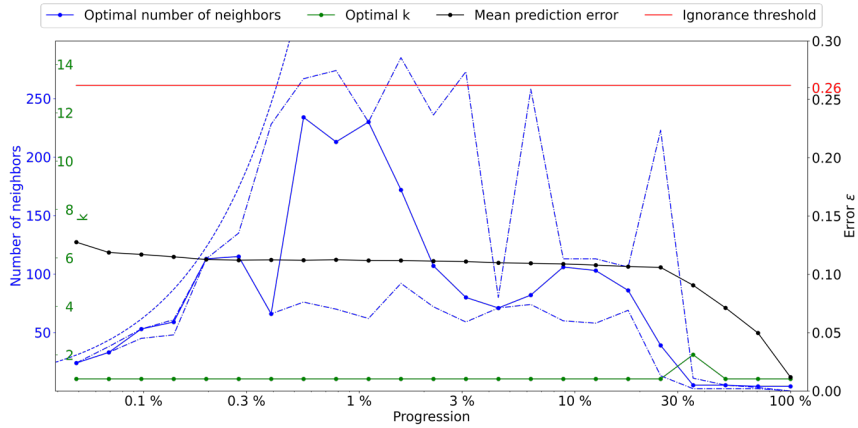
Field Code Changed

1111

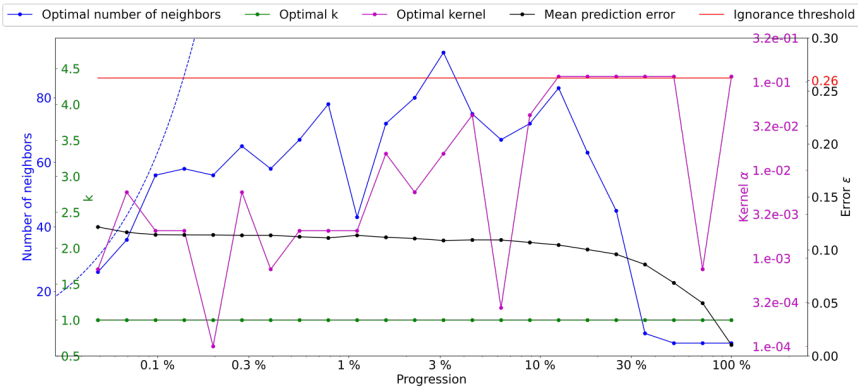
1112 Figure B.4 Benchmark between QS with adaptive kernel (Figure B.2) and uniform (without) kernel (Figure B.1)
 1113 over 100 simulations for 5 different metrics.

1114

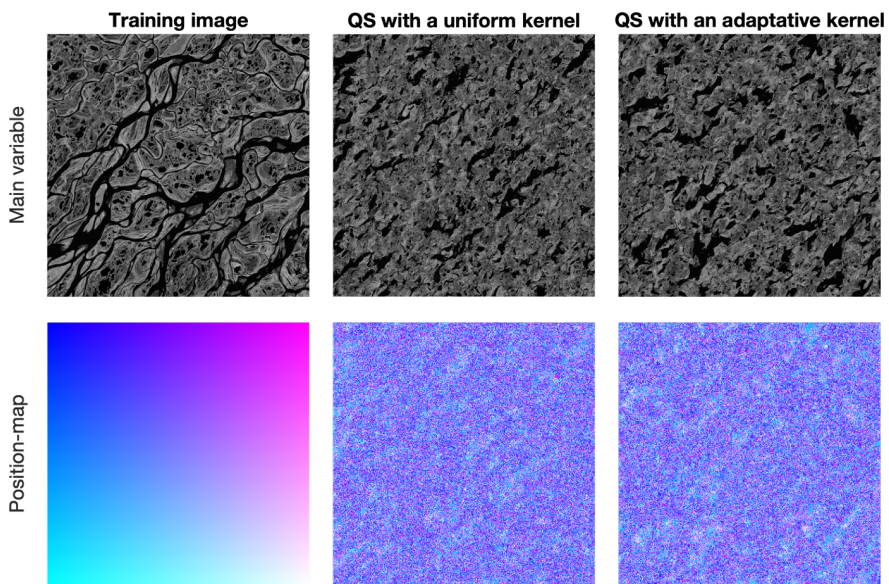
1118 C. Delta Lena (Mahmud et al., 2014)



1119
 1120 **Figure C.1 Optimal parameters for QS (k in green and number of neighbors in blue) as a function of the progression,**
 1121 **with the associated prediction error (in red). The red line represents the ignorance threshold. The dashed blue line is**
 1122 **the average density for the neighborhood considered. The dot-dashed line represents the variability in 1% of the error.**

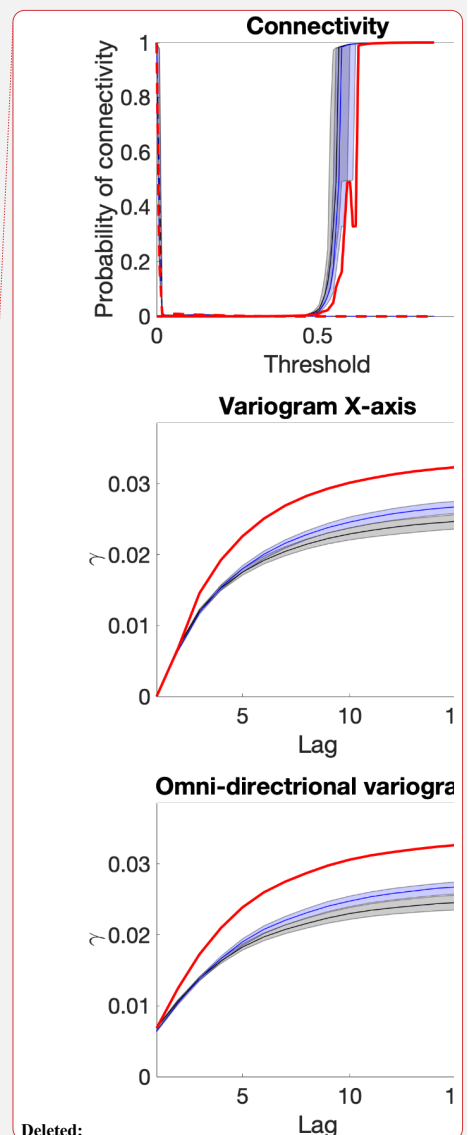
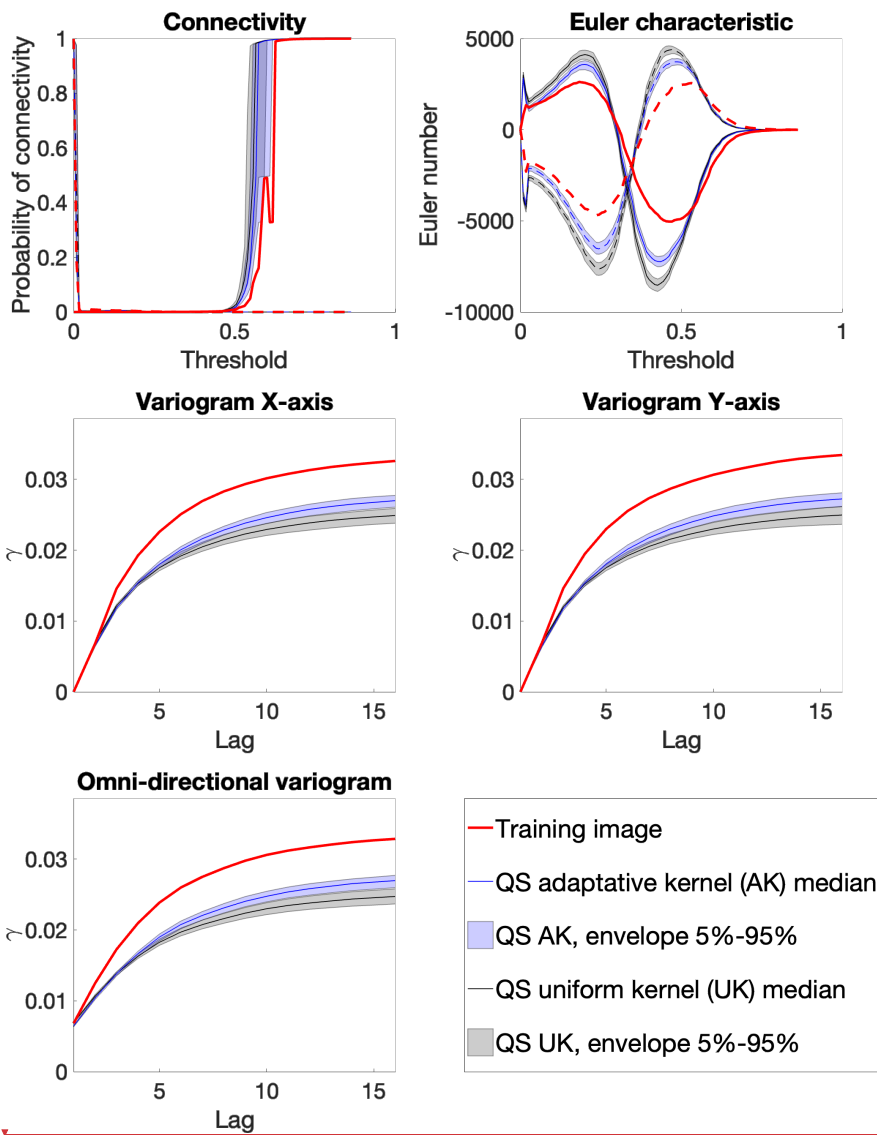


1123
 1124 **Figure C.2 Optimal parameters for QS (k in green and number of neighbors in blue, and the best kernel in magenta)**
 1125 **as a function of the progression, with the associated prediction error (in red). The dashed blue line is the average density**
 1126 **for the neighborhood considered.**



1127

1128 **Figure C.3** Simulation using QS using parameters generated by the automatic calibration.



Deleted:
 Deleted: Figure C.2
 Deleted: Figure C.1

1129
 1130 Figure C.4 Benchmark between QS with adaptative kernel (Figure C.2) and uniform (without) kernel (Figure C.1)
 1131 over 100 simulations for 5 different metrics.

1132